Supplementary Information

TGF-β-mediated crosstalk between TIGIT$^+$ Tregs and CD226$^+$CD8$^+$ T cells in the progression and remission of type 1 diabetes

Ting Zhong[1#], Xinyu Li[1#], Kang Lei[1#], Rong Tang[1], Qiaolin Deng[2], Paul Love[3], Zhiguang Zhou[1*], Bin Zhao[1, 4, 5*], Xia Li[1*]

[1]National Clinical Research Center for Metabolic Diseases, Key Laboratory of Diabetes Immunology, Ministry of Education, and Department of Metabolism and Endocrinology, The Second Xiangya Hospital of Central South University, Changsha, Hunan, China.

[2]Department of Physiology and Pharmacology, Karolinska Institute, 17177, Solna, Sweden.

[3]Section on Hematopoiesis and Lymphocyte Biology, Eunice Kennedy Shriver National Institute of Child Health and Human Development, National Institutes of Health, Bethesda, MD, United States.

[4]CSU-Sinocare Research Center for Nutrition and Metabolic Health, Xiangya School of Public Health, Central South University, Changsha, Hunan, China

[5]Furong Laboratory, Changsha, Hunan, China.

#These authors contributed equally to this manuscript.

*Corresponding authors: zhouzhiguang@csu.edu.cn (Zhiguang Zhou); binzhao@csu.edu.cn (Bin Zhao); lixia@csu.edu.cn (Xia Li).

This Supplementary Information File contains:

Supplementary Figures 1–18

Supplementary Table 1–8

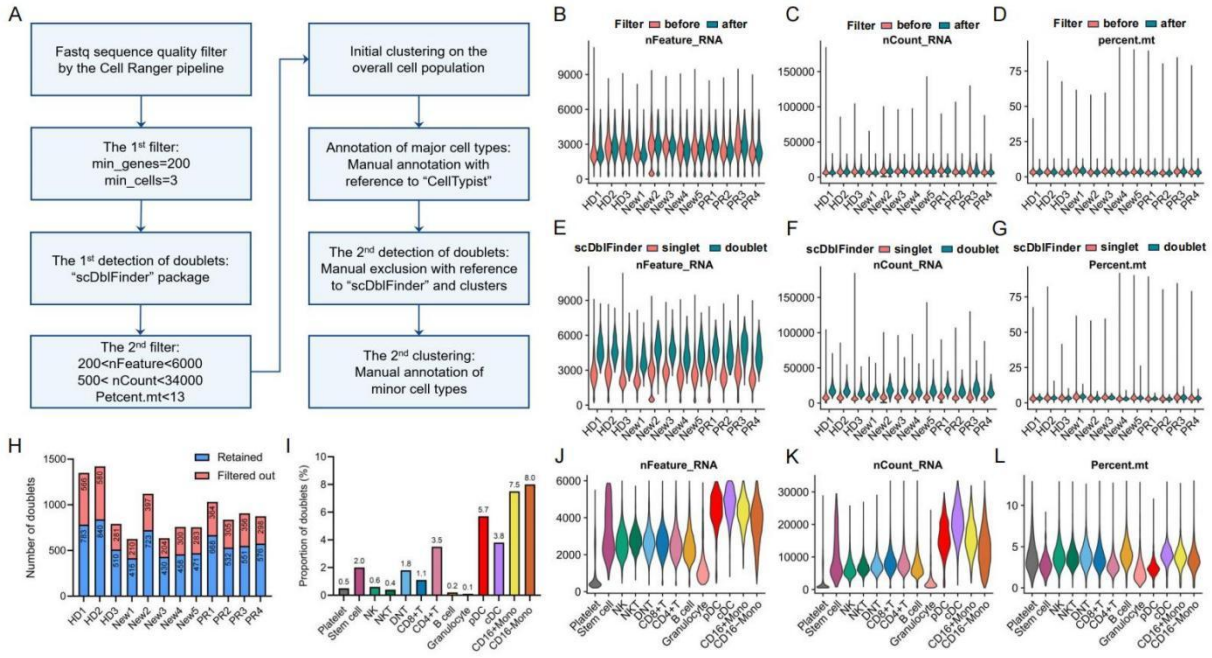

Supplementary Fig. 1 The quality control and cell annotation processes used in scRNA-seq data. (**A**) Flowchart illustrating the quality control and cell annotation processes used in scRNA-seq data. (**B–D**) Violin plots illustrating the comparison of various quality control metrics before and after the second round of filtration for each sample. These include key parameters such as the number of genes (**B**) UMI counts (**C**) and the percentage of mitochondrial genes (**D**). (**E–G**) Comparison of doublets and singlets identified by scDblFinder based on various quality control metrics. (**H**) The number of doublets removed in each sample after the second round of filtration. (**I**) The percentage of doublets in different cell types. (**J–L**) Violin plots comparing the quality control metrics after filtration across different cell types.

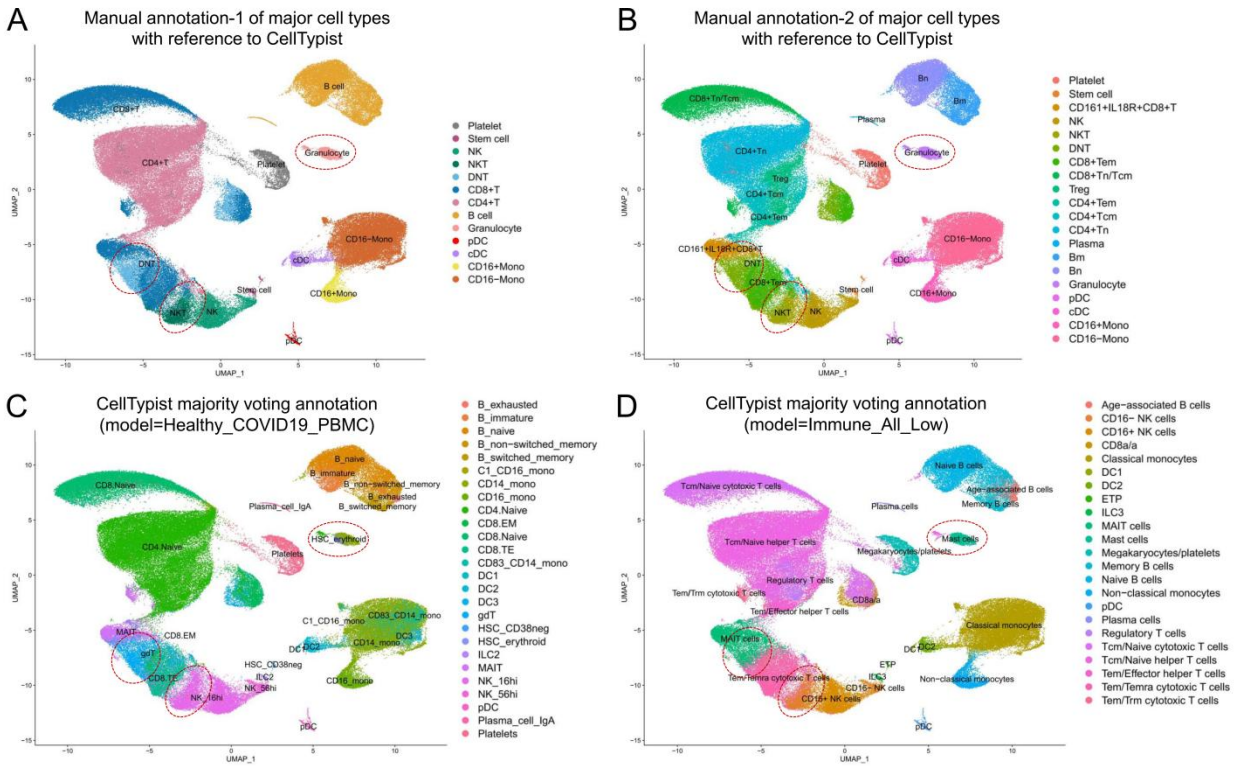

Supplementary Fig. 2 The annotation of major cell types. (**A**) The UMAP plot illustrates the manual annotation of major cell types guided by CellTypist. (**B**) The UMAP plot highlights the more refined classification of major cell types guided by CellTypist. (**C**) The UMAP plot illustrates the cell annotation results performed in CellTypist based on "Healthy_COVID19_PBMC" model. (**D**) The UMAP plot illustrates the cell annotation results performed in CellTypist based on "Immune_All_Low" model.

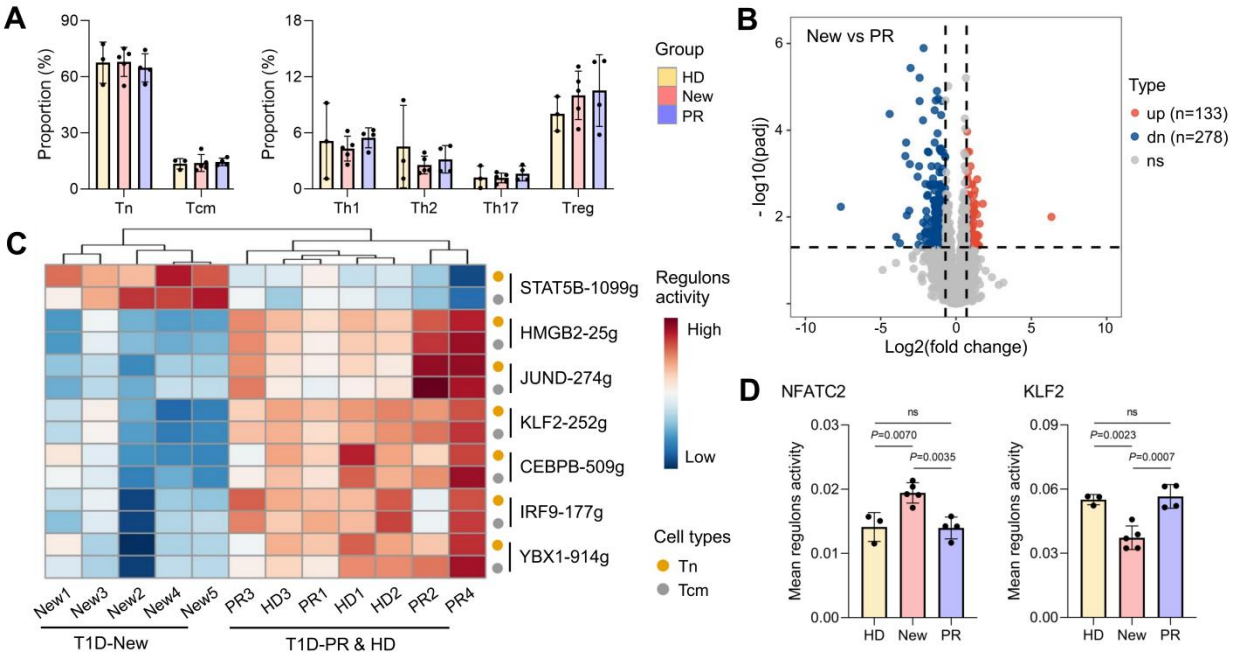

Supplementary Fig. 3 Differential gene analysis of CD4$^+$ T cell subsets. (**A**) Comparison of cell proportions within groups in CD4$^+$ T clusters. (**B**) Volcano plots showing the DEGs between groups in CD4$^+$ T cells calculated by pseudobulk analysis. Genes with log2FC >0.8 and adjusted *p* value <0.05 were defined as DEGs. (**C**) Heatmap representing the scaled values for the regulon activation ratios in Tn and Tcm cells among the individuals and groups. (**D**) Comparison of mean regulons activity among groups in Th1 cells. *P* values were calculated using a two-tailed t-test. Data are represented as mean ± SD. Source data are provided as a Source Data File.

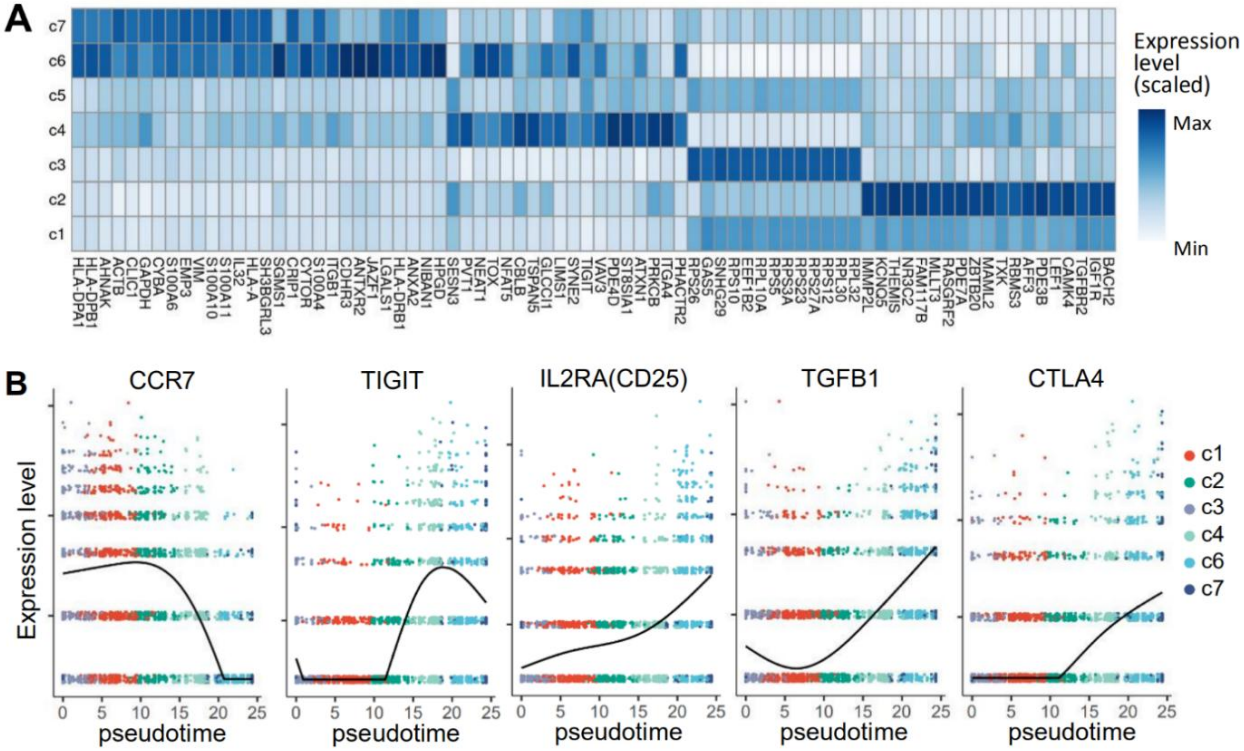

Supplementary Fig. 4 Gene expression characteristics of each Treg cluster. (A) Heatmap showing the scaled mean expression values for the top DEGs in each Treg subcluster. (**B)** Expression patterns of the functional genes in the different Treg subclusters ordered according to pseudotime. DEGs, differentially expressed genes.

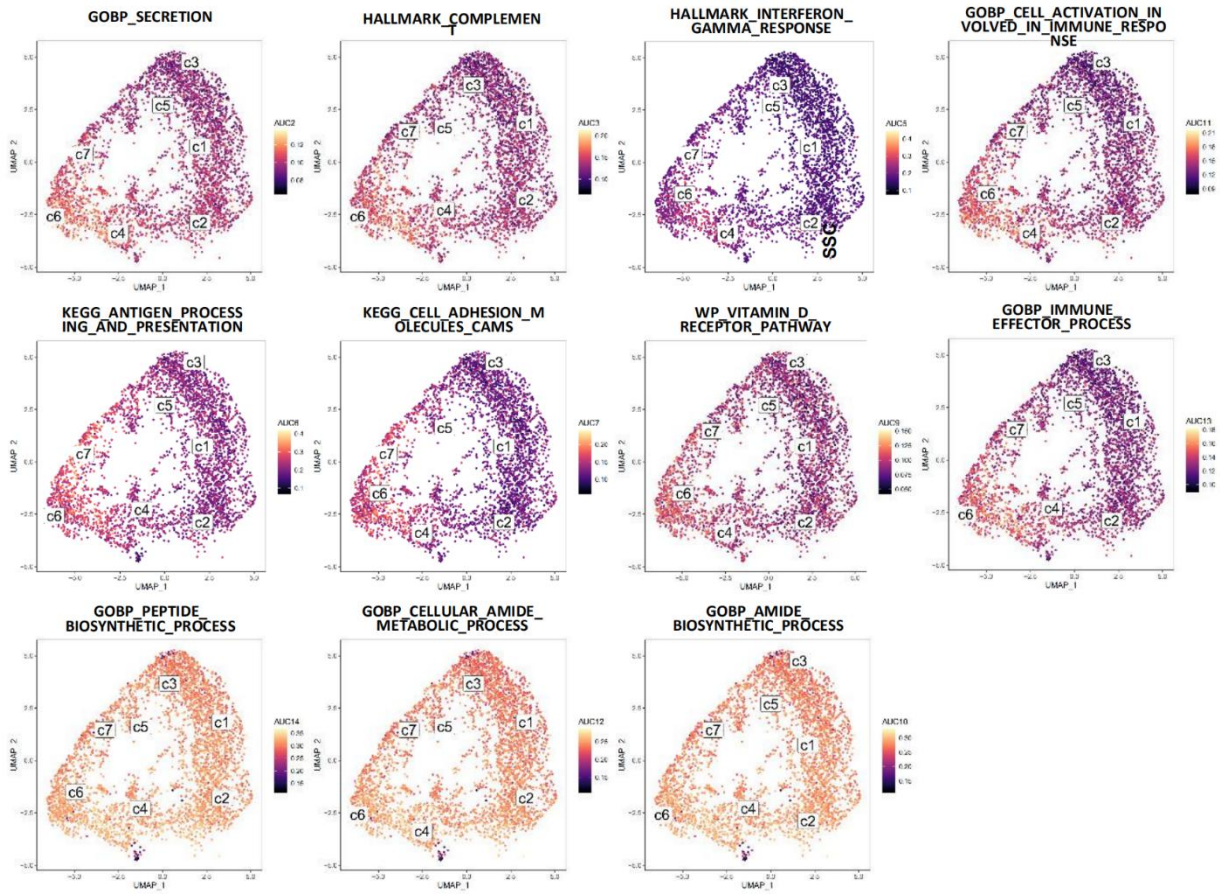

Supplementary Fig. 5 Heatmap showing the scaled mean AUC values for the pathways in the UMAP space.

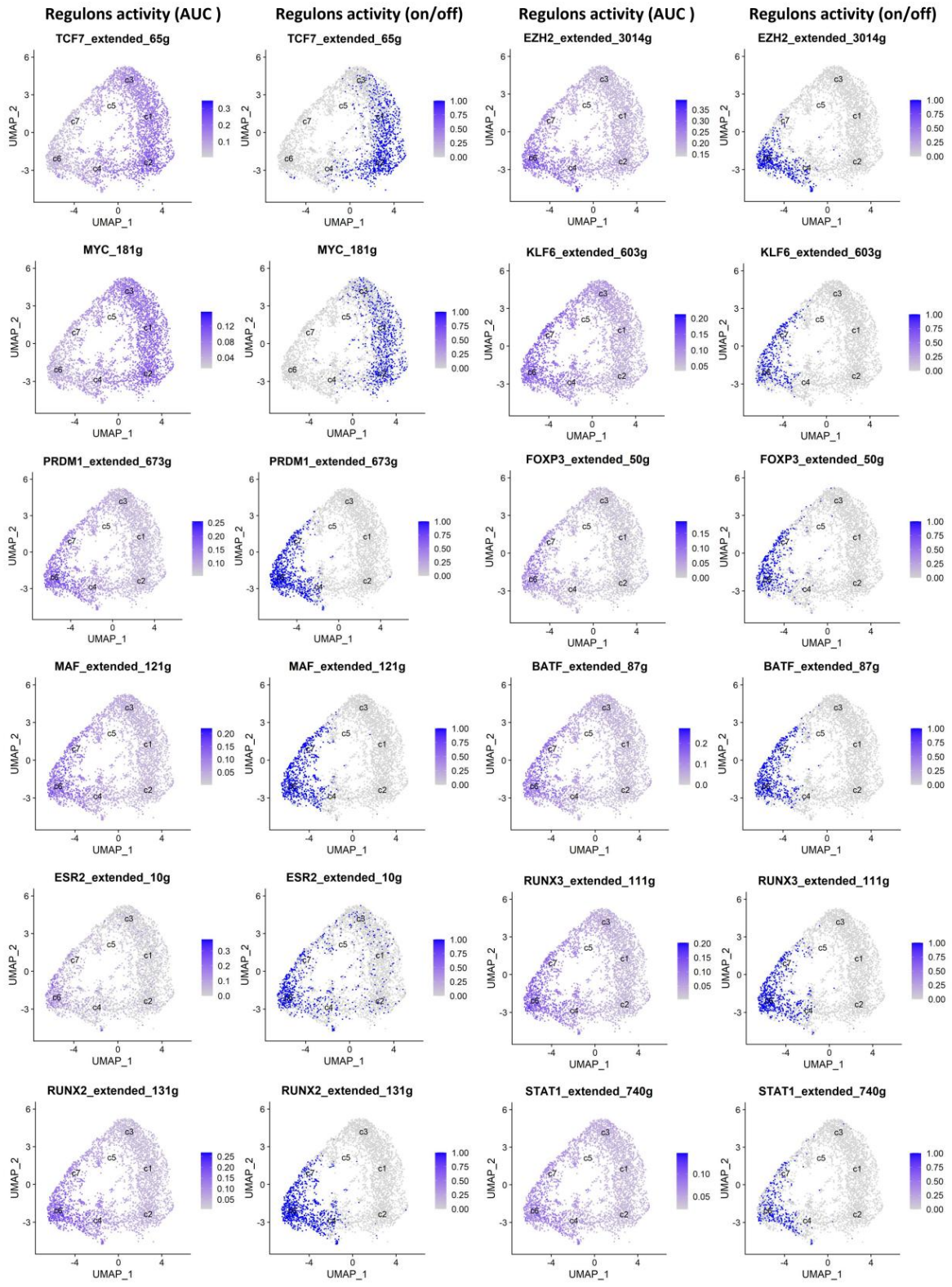

Supplementary Fig. 6 UMAP plots showing the activity of the regulons in the form of continuous (AUC, left) and dichotomous (on/off, right) variables.

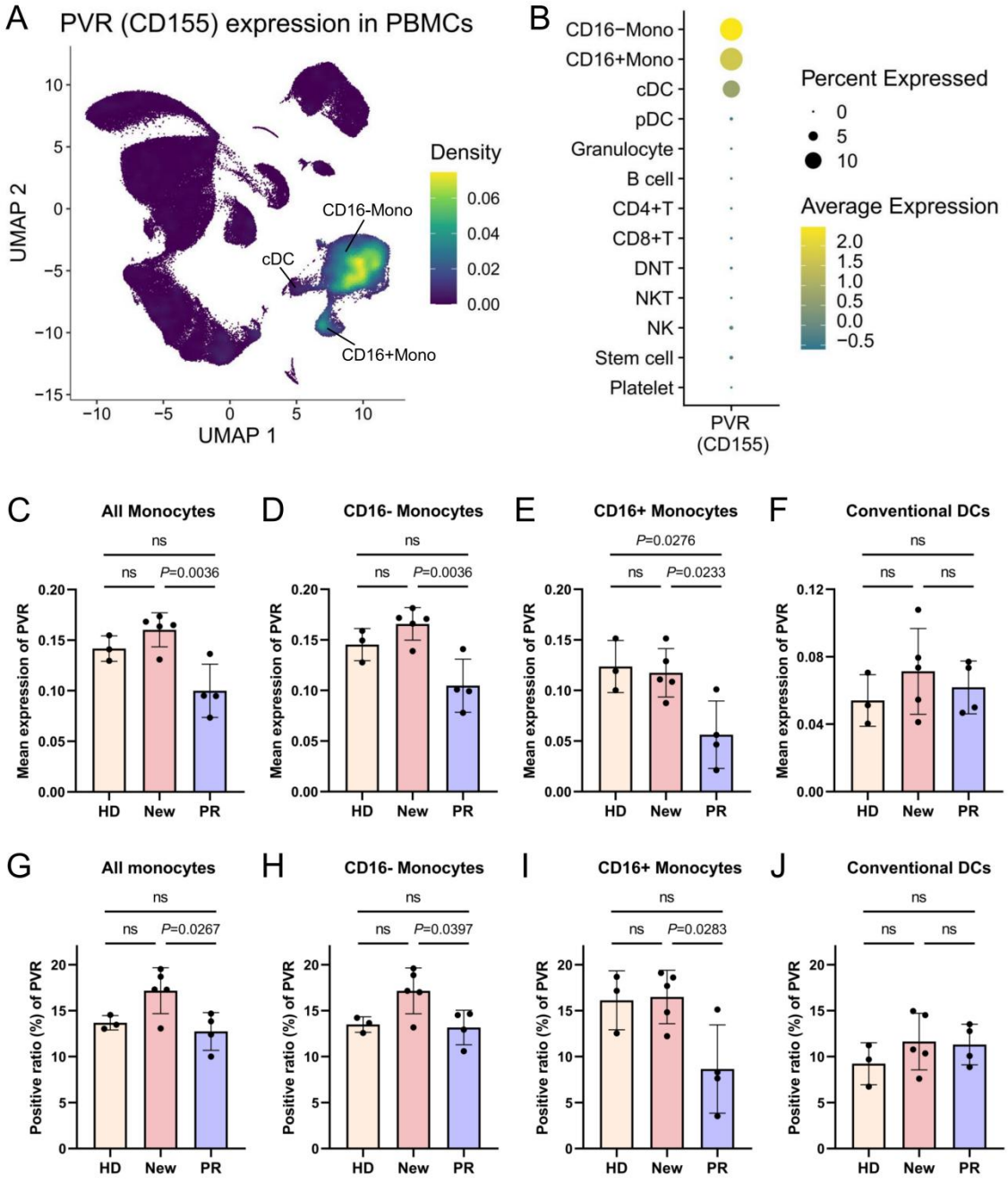

Supplementary Fig. 7 The expression of CD155. (**A**) The UMAP plot highlights the expression levels of PVR in PBMCs. (**B**) Dot plot showing the expression levels of the PVR in each cell type. (**C–F**) Comparisons of the mean PVR expression among the three groups in (**C**) all monocytes, (**D**) CD16− monocytes, (**E**) CD16+ monocytes, and (**F**) conventional DCs. (**G–J**) Comparisons of the positive ratio of PVR among the three groups in (**G**) all monocytes, (**H**) CD16− monocytes, (**I**) CD16+ monocytes, and (**J**) conventional DCs. *P* values were calculated using a two-tailed t-test. Data are presented as the mean ± SD. PVR, poliovirus receptor; PBMC, peripheral blood mononuclear cell. n indicates the number of biologically independent samples examined. Source data are provided as a Source Data File.

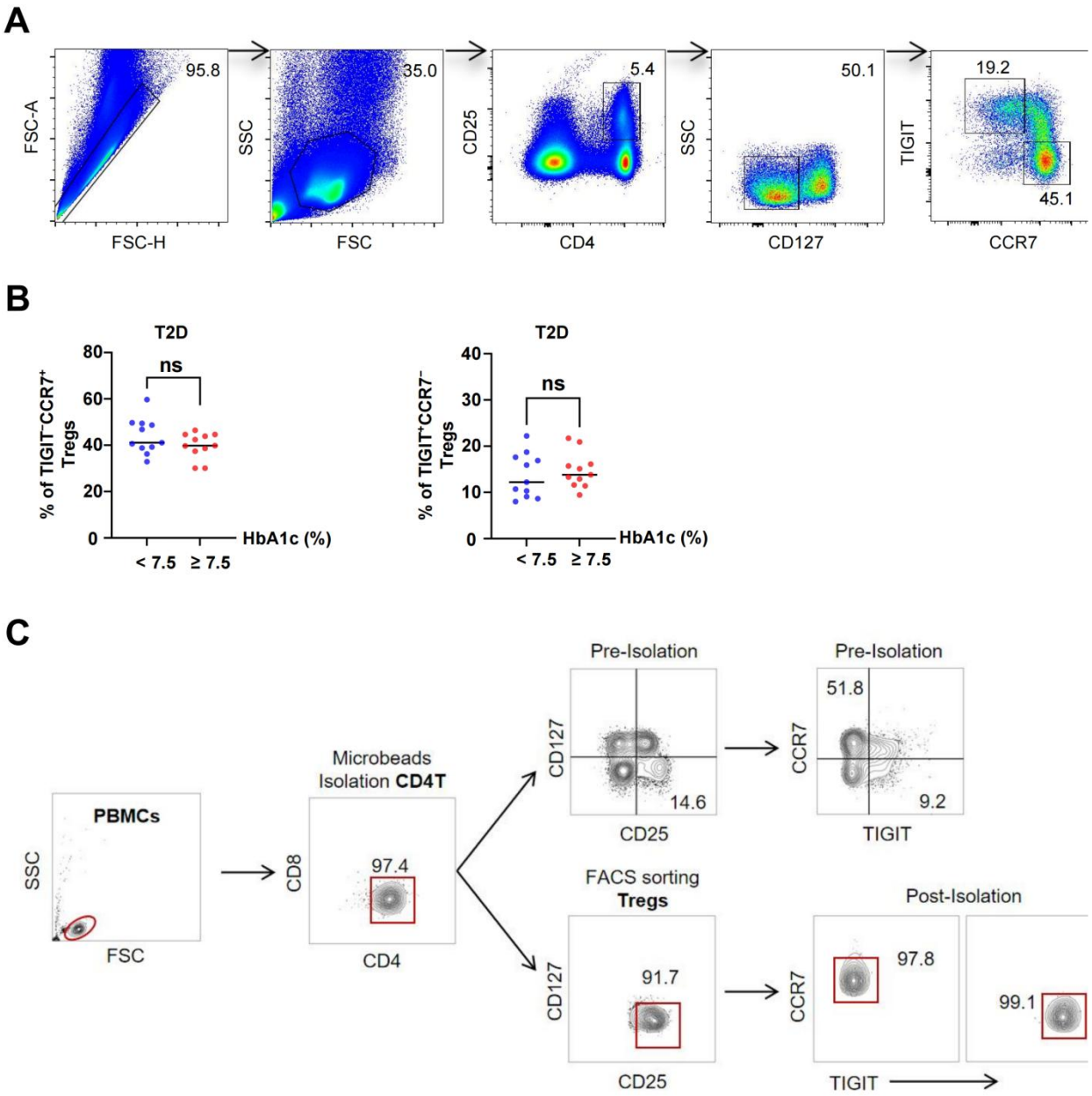
A
FSC-A
FSC-H
95.8
SSC
FSC
35.0
CD25
CD4
5.4
SSC
CD127
50.1
TIGIT
CCR7
19.2
45.1
B
T2D
ns
% of TIGIT⁻CCR7⁺ Tregs
HbA1c (%)
< 7.5
≥ 7.5
T2D
ns
% of TIGIT⁺CCR7⁻ Tregs
HbA1c (%)
< 7.5
≥ 7.5
C
PBMCs
SSC
FSC
Microbeads
Isolation CD4T
CD8
CD4
97.4
FACS sorting
Tregs
Pre-Isolation
CD127
CD25
14.6
Pre-Isolation
CCR7
TIGIT
51.8
9.2
CD127
CD25
91.7
Post-Isolation
CCR7
TIGIT
97.8
99.1
D
KI67
MFI
24000
20000
16000
12000
8000
8000
0
P=0.0001
P=0.0166
P=0.0259
P=0.0351
1:1
1:2
1:4
1:8
0:1
Tregs:Responder T
TIGIT⁺CCR7− Treg
TIGIT⁻CCR7⁺ Treg

Supplementary Fig. 8 The comparison and sorting process of the Treg subsets. (A) Gating strategy for the $TIGIT^{-}CCR7^{+}$ and $TIGIT^{+}CCR7^{-}$ Treg populations. (B) Comparison of the $TIGIT^{-}CCR7^{+}$ (left) and $TIGIT^{+}CCR7^{-}$ (right) Treg frequencies between two groups of T2D patients: HbA1c <7.5% (n=11, blue dot) and HbA1c 7.5% (n=11, red dot). Two-tailed unpaired t-test; data are shown as the mean ± SD. (C) Sorting process of Treg subsets. (D) Suppression assay of Treg subsets. $TIGIT^{+}CCR7^{-}$ Treg cells and $TIGIT^{-}CCR7^{+}$ Treg cells (5×10^{4}), isolated from T1D patients (n=6), were cocultured with autologous $CD8^{+}$ T cells in the presence of α-CD3/CD28 antibodies (0.5 bead/cell) for 48 h at 37°C. Ki-67 in $CD8^{+}$ T cells was measured. The triangle symbolizes the control group with a Tregs-to-Responder T ratio of 0:1. Two-tailed unpaired t-test; data are shown as the mean ± SEM. T2D, type 2 diabetes; and HbA1c, glycated hemoglobin. n indicates the number of biologically independent samples examined. Source data are provided as a Source Data File.

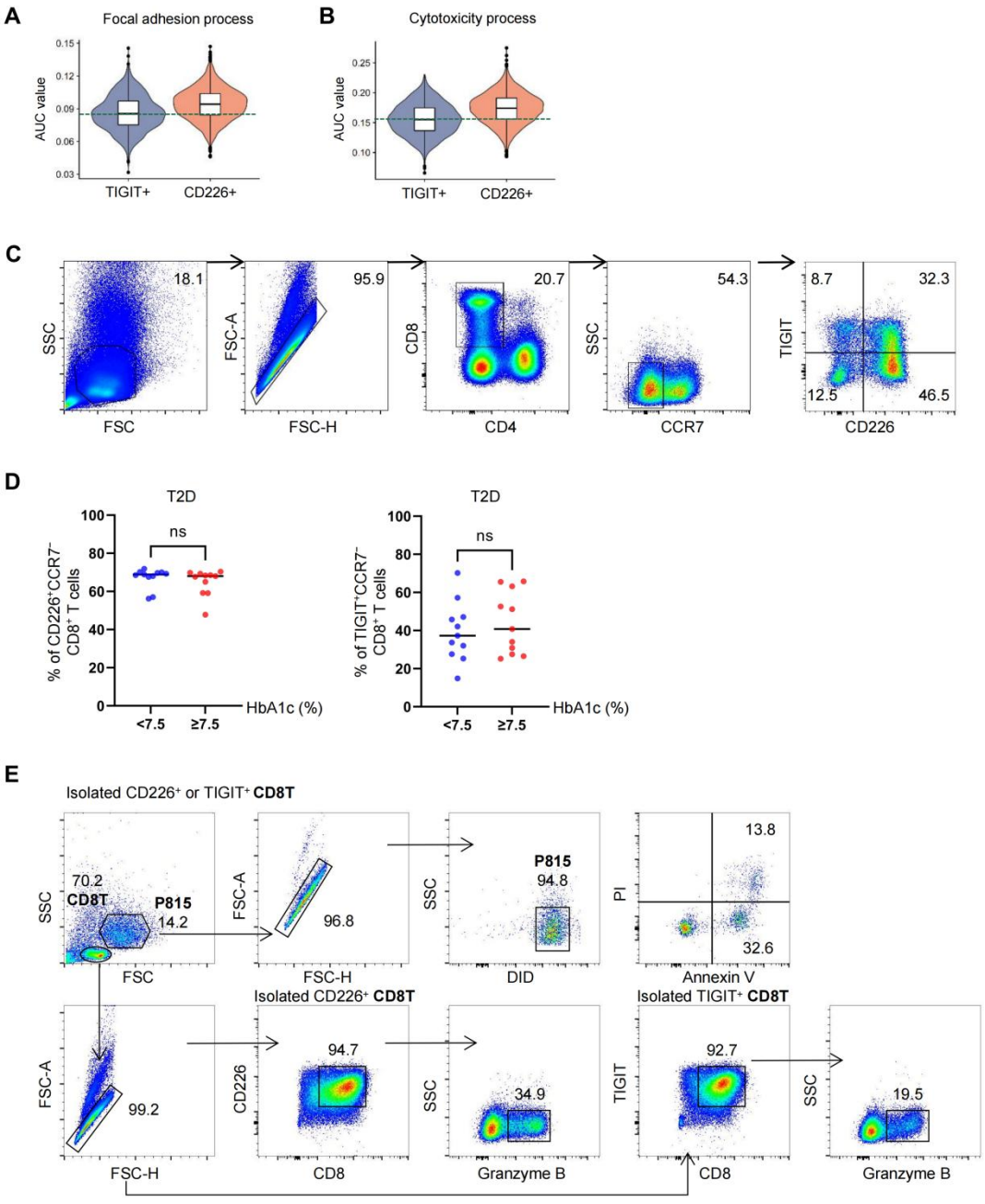

Supplementary Fig. 9 Comparison of the CD8$^+$ T cell subsets within T2D patients and gating strategies used for cell sorting. (**A–B**) Violin plot showing the differential pathway activities in CD226$^+$ and TIGIT$^+$CCR7$^-$CD8$^+$ T cells. **(C)** Gating strategy of CD226$^+$ and TIGIT$^+$CCR7$^-$CD8$^+$ T-cell populations. **(D)** Comparison of the frequencies of the CD226$^+$ (left) and TIGIT$^+$ (right) CCR7$^-$CD8$^+$ T cells between two groups of T2D patients: HbA1c <7.5% (n=11, blue dot) and HbA1c ≥7.5% (n=11, red dot). **(E)** Gating strategy to sort CD226$^+$/TIGIT$^+$CD8$^+$ T cells from PBMCs for in vitro cultures presented on Fig. 5K, L. *P* values were calculated using the two-tailed t-test. T2D, type 2 diabetes; HbA1c, glycated hemoglobin. n indicates the number of biologically independent samples examined. Source data are provided as a Source Data File.

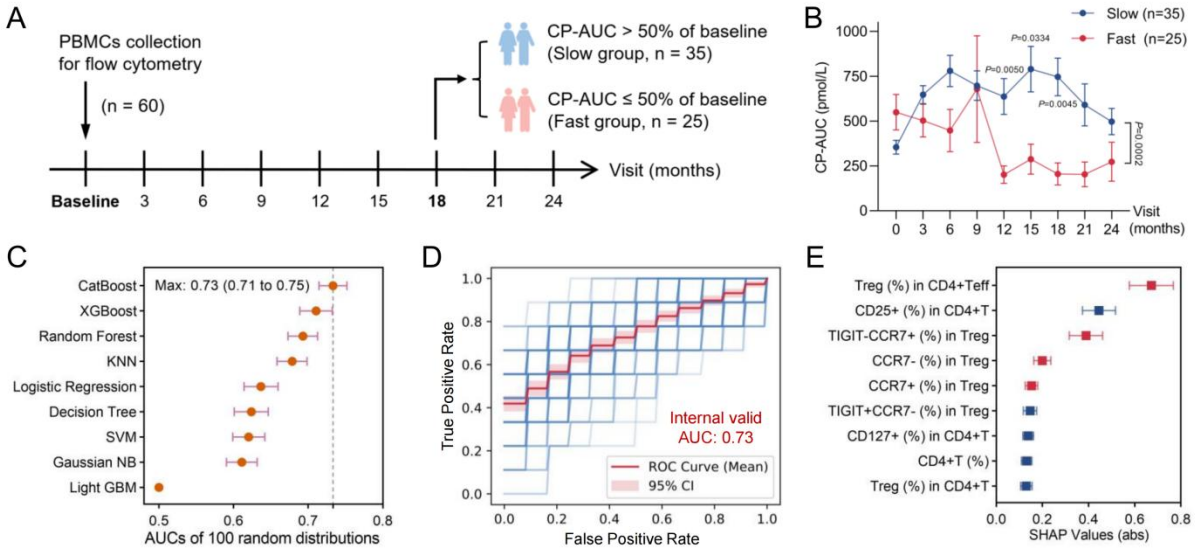

Supplementary Fig. 10 Machine learning reveiled a role of TIGIT^{+}CCR7^{-} Tregs in T1D progression. (**A**) Study design and cohort details for machine learning model development. **(B)** Temporal evolution of CP-AUC values in the discovery cohort of T1D patients. *P* were analyzed using mixed-effects model; data are shown as the mean ± SEM. **(C)** The comparative analysis of several machine learning algorithm models. **(D)** The blue solid line shows the ROC curve of the SVM classifier over multiple random samples in the internal validation dataset. The red solid line represents the average ROC curve of all random sampling experiments, while the shaded area denotes the 95% confidence interval. (**E**) The mean absolute SHAP values for a particular feature across all samples assesses the average contribution of that feature. The higher the mean absolute SHAP value, the more significant the feature's contribution to the model prediction of the entire dataset. Positive SHAP values (shown in red) indicate that the feature has a positive impact on the model's predictions, and vice versa. n indicates the number of biologically independent samples examined. Source data are provided as a Source Data File.

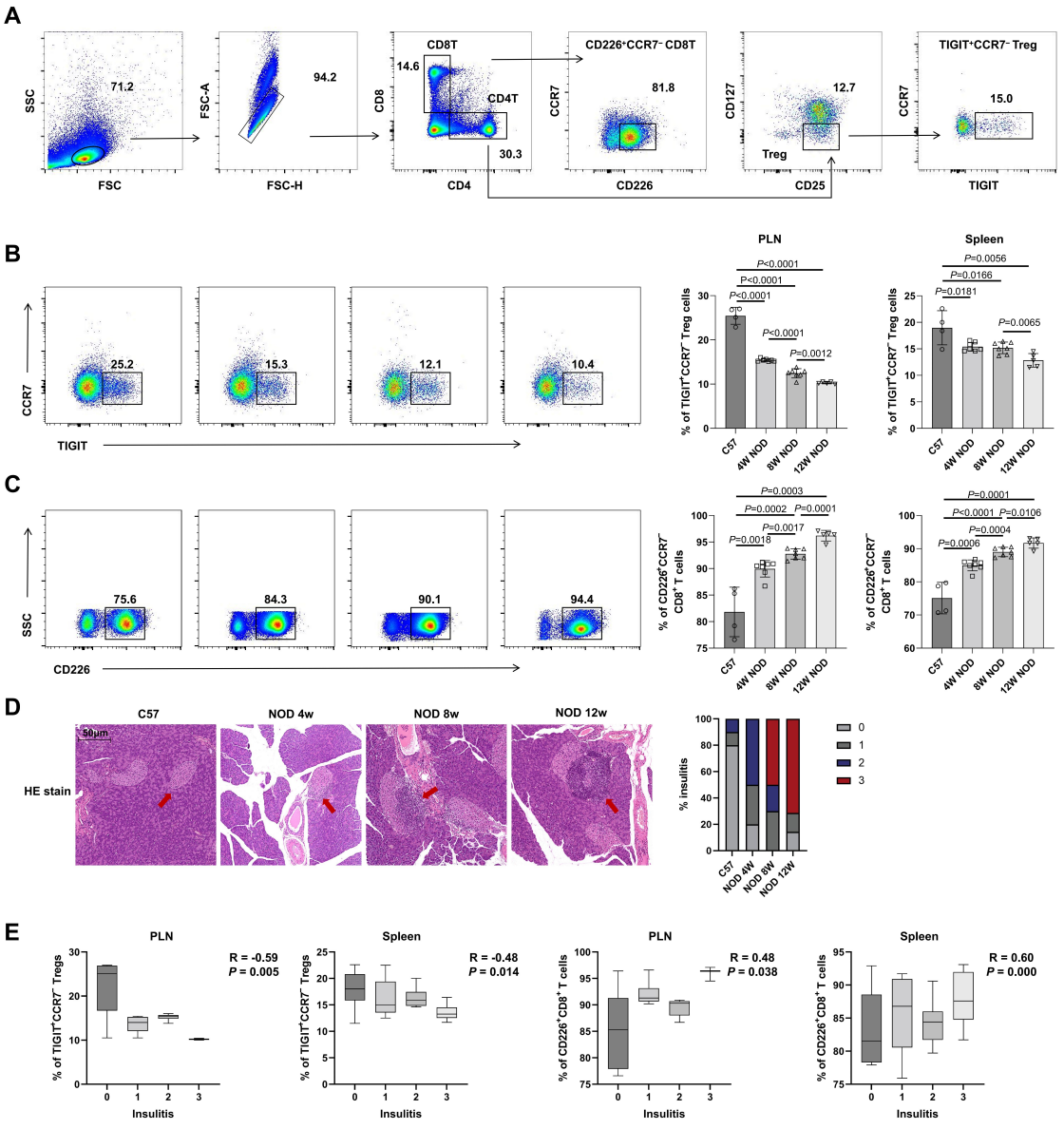

Supplementary Fig. 11 Alterations in TIGIT$^+$CCR7$^-$ Tregs and CD226$^+$CCR7$^-$CD8$^+$ T cells in NOD mice. (A) Gating strategy to determine the percentage of TIGIT$^+$CCR7$^-$ Tregs and CD226$^+$CCR7$^-$CD8$^+$ T cells in NOD mice. (**B–C**) Representative flow cytometry plots and quantification for (**B**) TIGIT$^+$CCR7$^-$ Tregs, and (**C**) CD226$^+$CCR7$^-$CD8$^+$ T cells in PLN and spleen of 4- (n=7), 8- (n=7), and 12-week-old NOD mice (n=5), compared with C57 controls (n=4). Symbols represent each group: C57 mice (circles), 4-week NOD mice (squares), 8-week (upright triangles), and 12-week NOD mice (inverted triangles). *P* values were calculated using a two-tailed t-test. (**D**) HE staining in four groups. Insulitis scoring across the four groups (n=7) is depicted as follows: Grade 0, no lymphocytic infiltration (grey bars); grade 1, <30% infiltration (dark grey bars); grade 2, <50% islet infiltration (blue bars); grade 3, >50% islet infiltration (red bars). (**E**) Box plots showing the association between T cell subsets and the severity of insulitis. *P* values were calculated using Spearman's correlation analysis. n indicates the number of biologically independent samples examined. Source data are provided as a Source Data File.

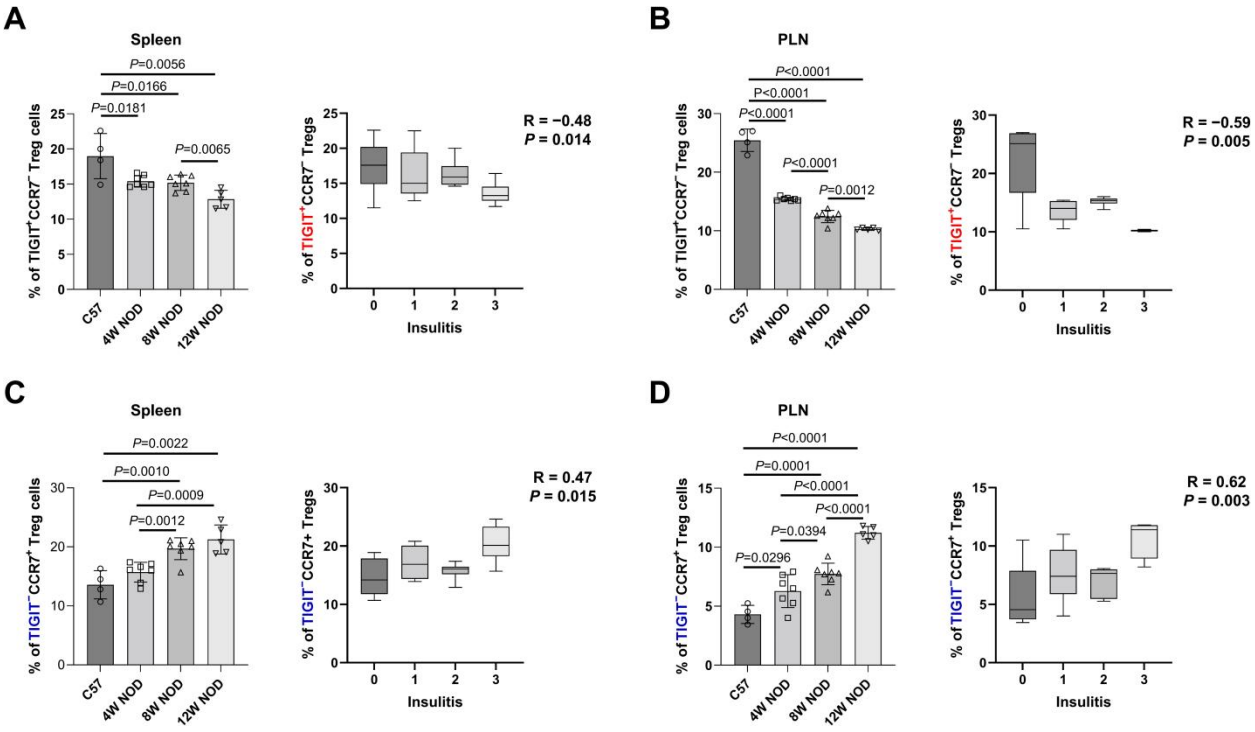

Supplementary Fig. 12 Dynamics of TIGIT$^+$CCR7$^-$ versus TIGIT$^-$CCR7$^+$ Tregs in NOD mice. Association between TIGIT$^+$CCR7$^-$ Tregs (**A–B**) and TIGIT$^-$CCR7$^+$ Tregs (**C–D**) with the severity of insulitis in the spleen and PLN of NOD mice aged 4 (n=7), 8 (n=7), and 12 (n=5) weeks, compared to age-matched C57BL/6 controls (n=4). Symbols represent each group: C57BL/6 mice (circles), 4-week NOD mice (squares), 8-week (upright triangles), and 12-week NOD mice (inverted triangles). *P* values were calculated using a t-test or Spearman's correlation analysis. Data are presented as the mean ± SD. n indicates the number of biologically independent samples examined. Source data are provided as a Source Data File.

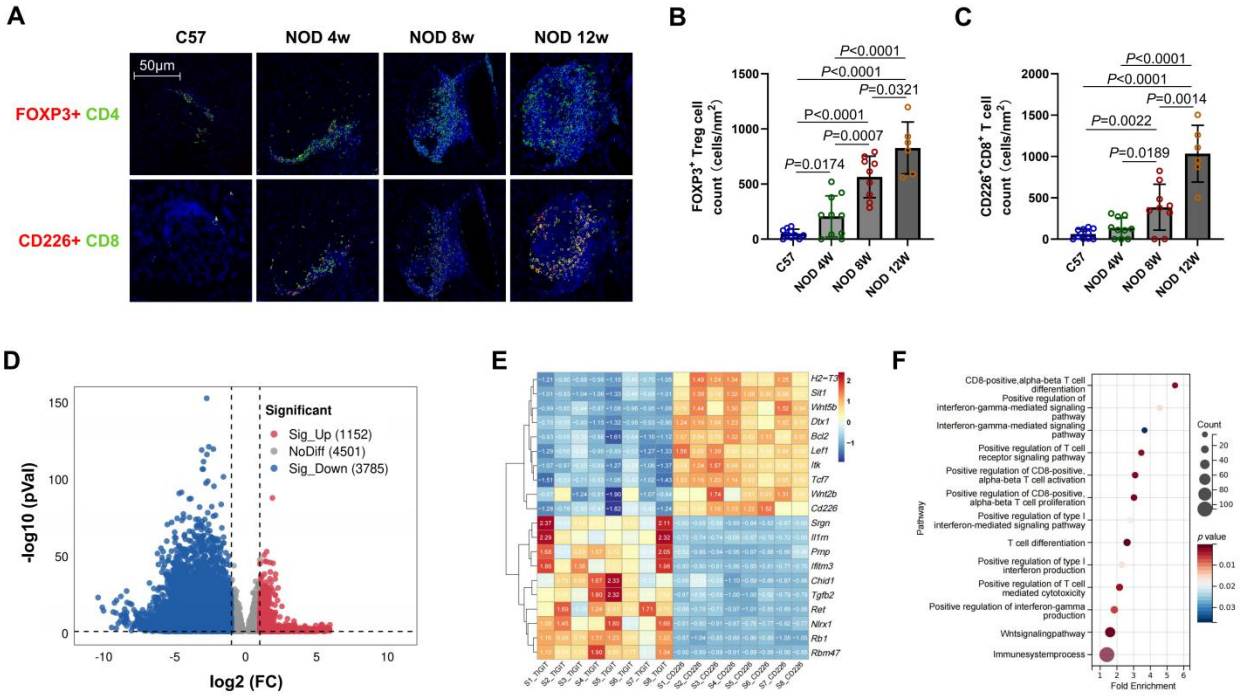

Supplementary Fig. 13 Cytotoxic CD226$^+$CD8$^+$ T cells accumulate locally in insulitis. (**A–C**) Multiplex fluorescence immunohistochemistry staining was used to evaluate the presence of CD226$^+$CD8$^+$ T cells within the islets of NOD mice at various ages. (**A**) Representative multiplex fluorescence images of Treg and CD226$^+$CD8$^+$ T cells in the pancreas specimen (n=10). Nuclei, CD4 and CD8, as well as FOXP3 and CD226 within the cells, are visualized in blue, green, and red, respectively. (**B**) FOXP3$^+$ Tregs were determined by cell density. (**C**) Assessment of the density of CD226$^+$CD8$^+$ T cells within the islets. (**D**) Volcano map and (**E**) heatmap showing the scaled expression of the top DEGs between TIGIT$^+$ and CD226$^+$CD8$^+$ T cells. (**F**) Bubble plot showing the upregulated pathways in CD226$^+$CD8$^+$ T cells. *P* values were calculated using the two-tailed t-test; data were shown as the mean ± SD. n indicates the number of biologically independent samples examined. Source data are provided as a Source Data File.

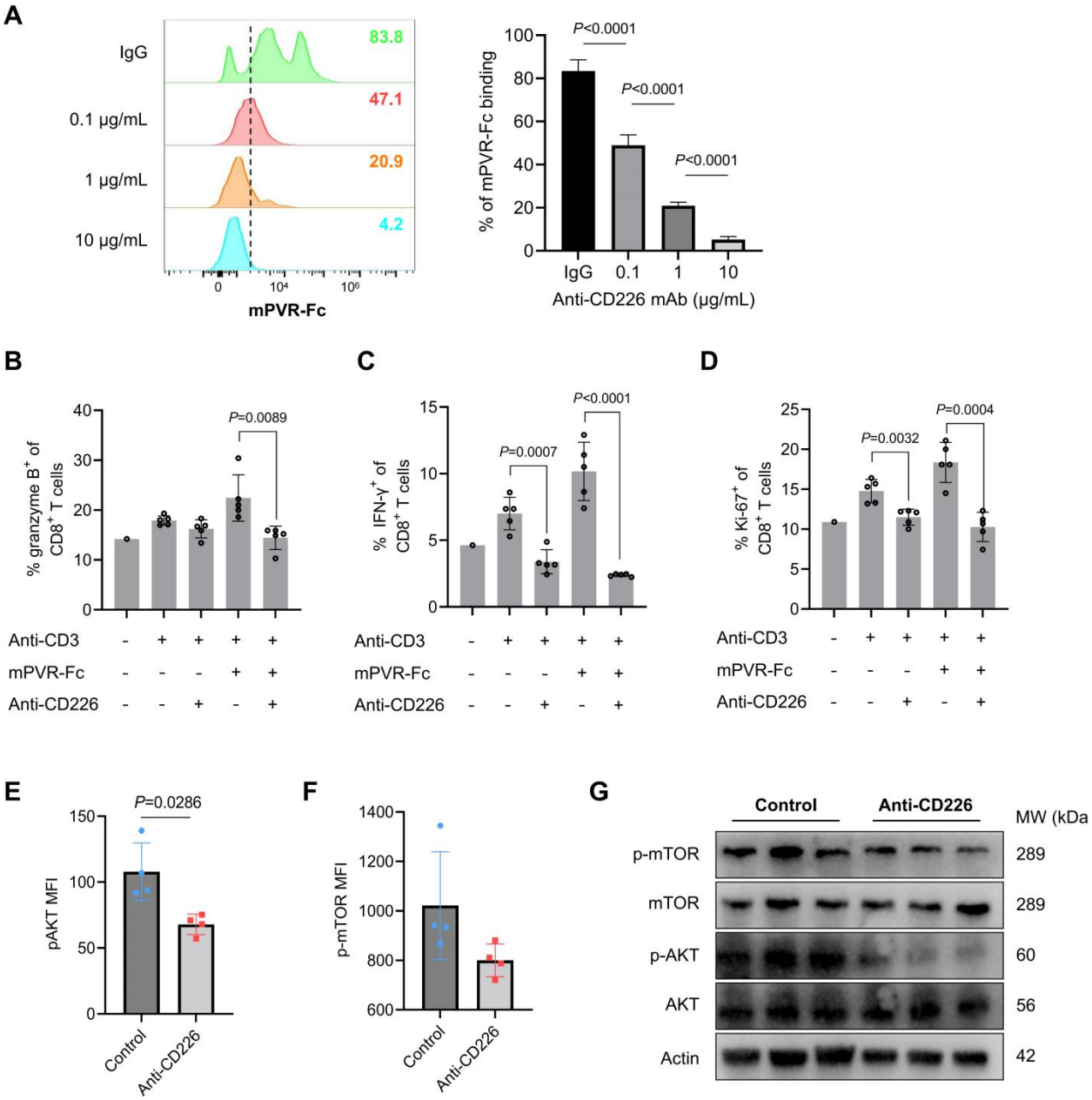

Supplementary Fig. 14 (related to Fig.8) CD226 blockade inhibited the proliferation and cytokine-production of CD8⁺ T cells. (**A**) Identification of rat anti-mouse CD226 monoclonal antibody. Representative histogram (left) and quantification (right) of mouse PVR-hFc fusion protein binding to mouse CD8⁺ T cells at indicated anti-mCD226 concentrations. (**B–D**) Splenic CD8⁺ T cells from NOD mice were enriched and stimulated for 24 h in the presence of anti-CD3 (5 μg/mL), mPVR-Fc (5 μg/mL), and/or anti-CD226 (5 μg/mL) antibodies as indicated. The expression levels of (**B**) granzyme B, (**C**) IFN-γ, and (**D**) Ki-67 within CD8⁺ T cells were shown (n=5). The expression levels of (**E**) pAKT, and (**F**) p-mTOR within splenic CD8⁺ T cells from Cy-induced mouse model were depicted (n=4). (**G**) CD8⁺ T cells from the spleens of the two groups were sorted and the levels of pAKT and p-mTOR were determined by western blots. Two-tailed unpaired t-test; data were shown as the mean ± SD. n indicates the number of biologically independent samples examined. Source data are provided as a Source Data File.

STZ-induced mouse model:

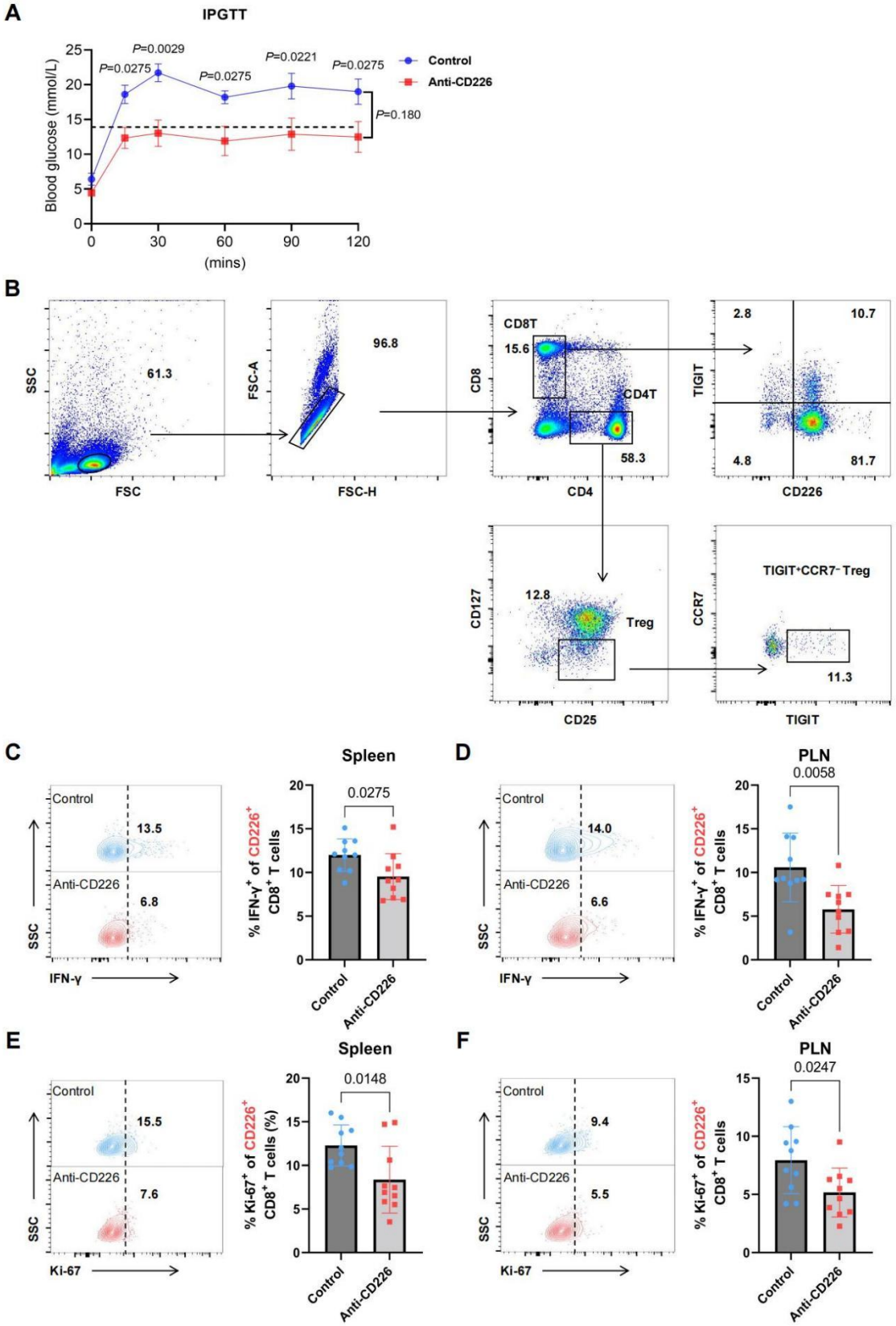

Supplementary Fig. 15 (related to Fig.8) Anti-CD226 treatment does change the function of CD226^{+}CD8^{+} T cells and glucose tolerance in STZ-induced diabetic mice. (**A**) Comparison of the IPGTT (n=5), analyzed via mixed-effects model; data are shown as the mean ± SEM. **(B)** Gating strategy to determine the percentage of TIGIT^{+}CCR7^{-} Tregs and CD226^{+}/TIGIT^{+}CD8^{+} T cells in STZ-induced diabetic mice. **(C–F)** The expression levels of (**C, D**) IFN-γ, and (**E, F**) Ki-67 within CD226^{+}CD8^{+} T cells in the spleen and PLN are depicted for the two groups (n=10). Two-tailed unpaired t-test; data are shown as the mean ± SD. n indicates the number of biologically independent samples examined. Source data are provided as a Source Data File.

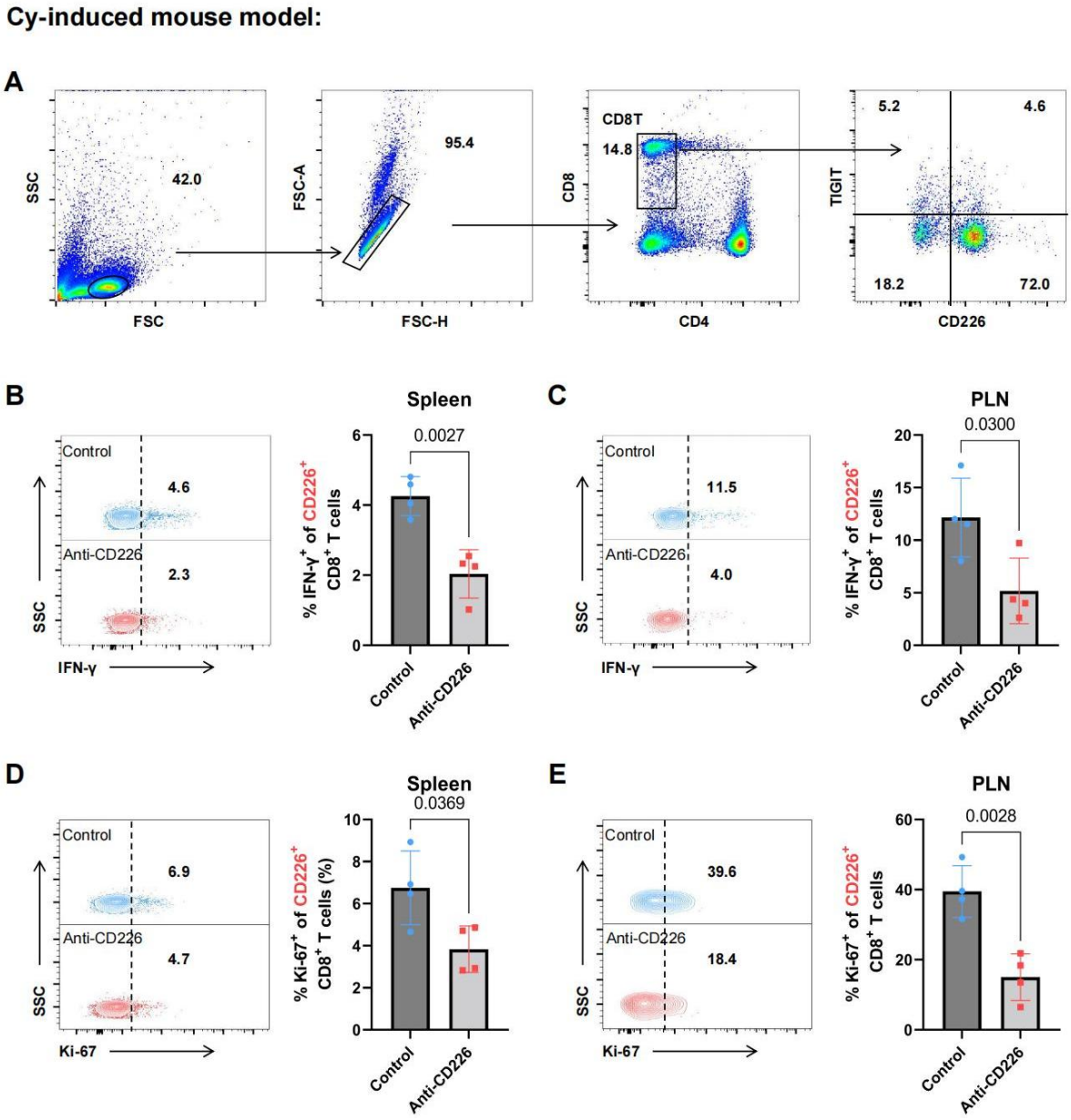

Supplementary Fig. 16 (related to Fig.8) Anti-CD226 treatment inhibited the proliferation and cytokine-production of CD226$^+$CD8$^+$ T cells in Cy-induced NOD mice. (A) Gating strategy to determine the percentage of CD226$^+$ and TIGIT$^+$CD8$^+$ T cells in Cy-induced NOD mice. **(B–E)** The expression levels of (**B, C**) IFN-γ, and (**D, E**) Ki-67 within CD226$^+$CD8$^+$ T cells in the spleen and PLN were depicted for the two groups (n=4). Two-tailed unpaired t-test; data were shown as the mean ± SD. n indicates the number of biologically independent samples examined. Source data are provided as a Source Data File.

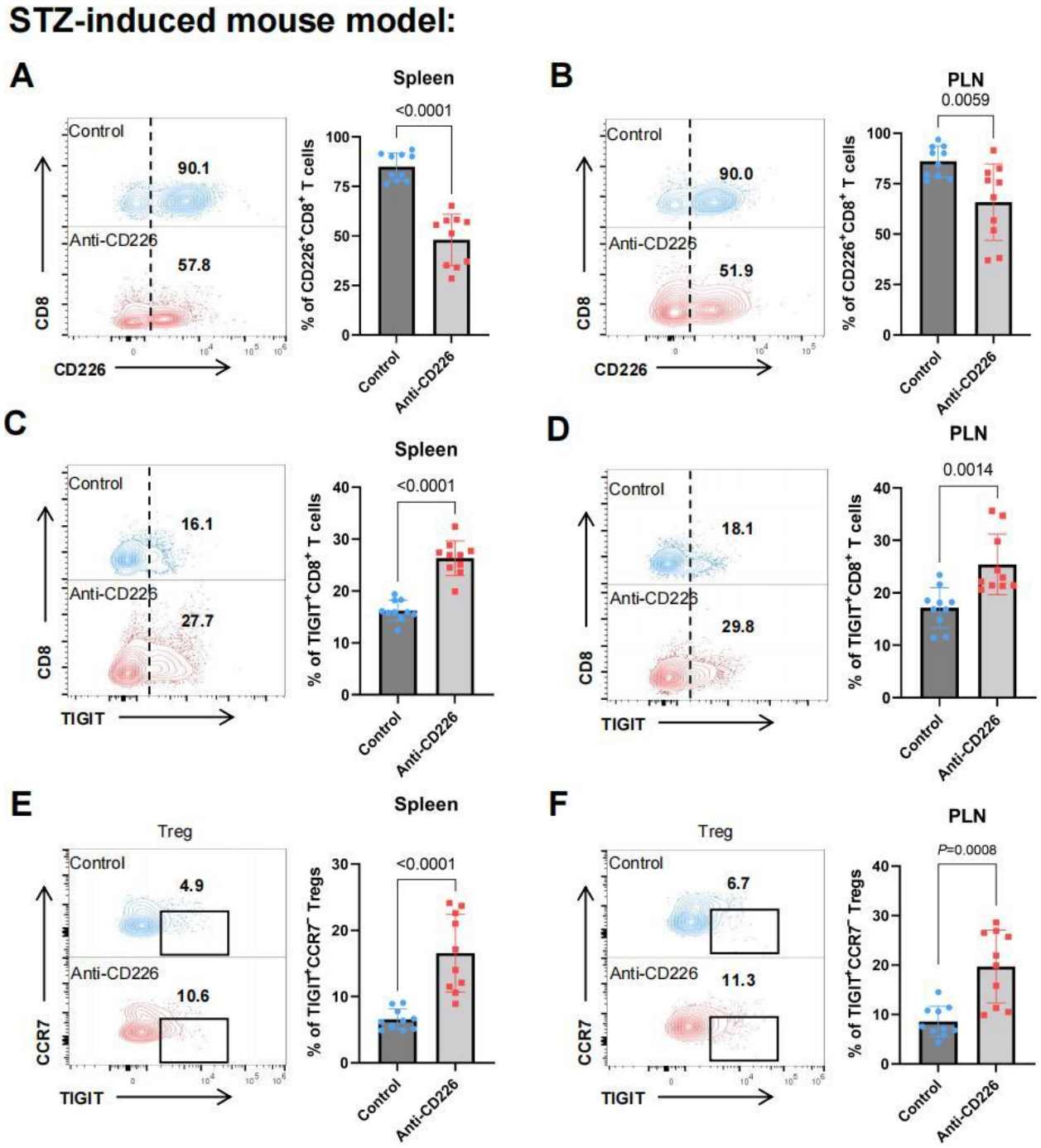

Supplementary Fig. 17 (related to Fig.8) Anti-CD226 therapy promotes immune equilibrium in STZ-induced diabetic mice. Male C57BL/6 mice (n=20/group) received STZ to induce diabetes. The Anti-CD226 group got 25 μg/mouse of the antibody every three days for four doses; controls had isotype injections. Post-treatment, five mice/group were analyzed for immune response; others were monitored for diabetes progression. (**A–F**) Frequencies of $CD226^+/TIGIT^+CD8^+$ T cells and $TIGIT^+$ Tregs in spleen and PLN are shown (n=10). *P* values were calculated using the two-tailed t-test; data were shown as the mean ± SD. T1D, type 1 diabetes; STZ, streptozotocin; PLN, pancreatic lymph nodes. n indicates the number of biologically independent samples examined. Source data are provided as a Source Data File.

Cy-induced mouse model:

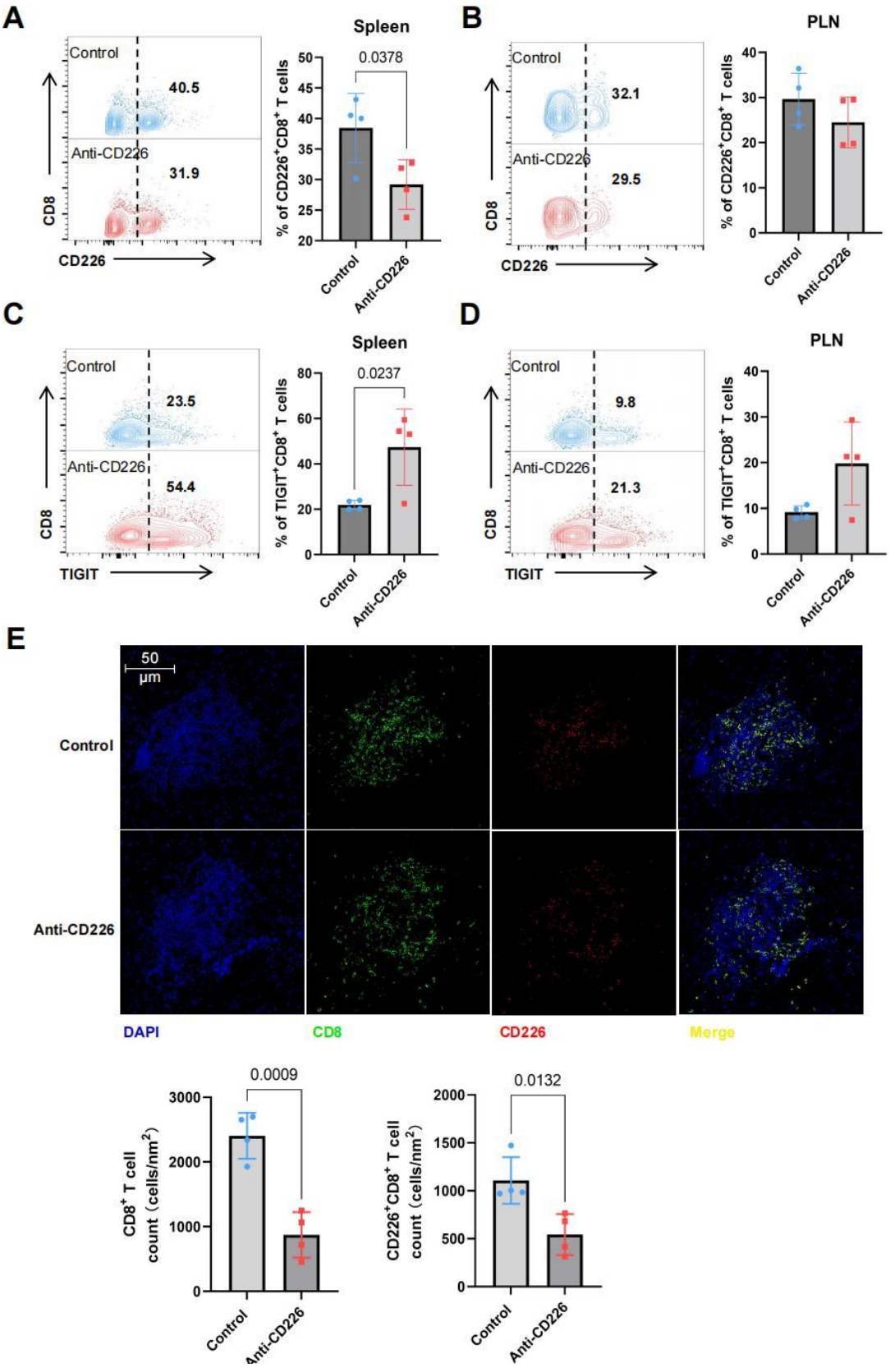

Supplementary Fig. 18 (related to Fig.8) Anti-CD226 therapy promotes immune equilibrium in Cy-induced NOD mice. Female NOD mice (n=8/group) received Cy to expedite diabetes. Post-anti-CD226 or isotype treatment, four were used for immune profiling; remaining mice were tracked for diabetes onset. (**A–D**) Frequencies of $CD226^+$/$TIGIT^+CD8^+$ T cells in spleen and PLN are shown (n=4). (**E**) Multiplex fluorescence immunohistochemistry staining was used to evaluate the presence of total $CD8^+$ T cells and $CD226^+CD8^+$ T cells within the islets of NOD mice. Representative multiplex fluorescence images in the pancreas specimen were shown. Nuclei, CD8 and CD226 within the cells, are visualized in blue, green, and red, respectively. Assessment of the density of total $CD8^+$ T cells and $CD226^+CD8^+$ T cells within the islets. *P* values were calculated using the two-tailed t-test; data were shown as the mean ± SD. T1D, type 1 diabetes; STZ, streptozotocin; PLN, pancreatic lymph nodes; Cy, cyclophosphamide; DAPI, diamidino-phenyl-indole. n indicates the number of biologically independent samples examined. Source data are provided as a Source Data File.

Supplementary Table 1

Single cell sequencing sample data

Sample name	Group	Batch	Number of Reads	Vaild Barcodes	Q30 Bases in Barcode	Q30 Bases in RNA Read	Q30 Bases in UMI	Estimated Barcode Count	Estimated Barcode UMI Count	Median Counts per cell	Median UMI Counts per cell	Sequencing saturation (%)	Total Genes Detected	Median Genes per cell
HD1	HD	Batch6	703061558	98.4%	97.6%	93.8%	97.5%	12112	106674955	58046	6953	78.9%	27999	2324
HD2	HD	Batch6	602727175	98.1%	95.5%	92.1%	95.1%	18699	176134089	32233	8028	59.7%	28879	2806
HD3	HD	Batch7	604065136	98.2%	95.5%	92.3%	95.1%	17685	170989177	34156	8219	61.2%	28714	2736
New1	New	Batch1	627142447	98.2%	96.2%	92.0%	96.0%	9783	72156657	64105	6412	84.4%	27004	2217
New2	New	Batch2	608638840	97.5%	95.8%	92.3%	95.4%	15493	149276233	39284	8464	62.5%	29111	2911
New3	New	Batch3	734083586	98.1%	96.7%	93.4%	96.6%	9384	91774252	78227	8609	80.6%	27667	2899
New4	New	Batch4	685458699	97.9%	96.3%	92.7%	96.0%	10214	90699430	67109	7756.5	79.1%	28226	2546
New5	New	Batch4	689669054	97.8%	96.3%	92.6%	96.0%	10800	104267764	63858	8312.5	76.9%	28401	2641
PR1	remission	Batch5	714897267	97.8%	96.8%	93.3%	96.5%	14527	142372709	49211	9130	72.1%	28571	2910
PR2	remission	Batch8	656604731	96.5%	96.4%	88.4%	95.9%	10636	101543337	61734	7821	76.2%	28566	2529
PR3	remission	Batch8	699195981	97.7%	96.7%	88.8%	96.1%	11687	126571135	59826	8874	75.2%	28669	3039
PR4	remission	Batch8	754799761	96.2%	96.6%	88.4%	96.0%	12591	116587466	59947	7373	74.5%	29106	2449

Abbreviations: HD, heathy donor; New, new-onset cases with T1D; remission, T1D cases in the partial remission phase.

Supplementary Table 2

Genes that characterize cell types

Cell	**Markers**
B	CD79A, MS4A1, CD19
$CD16^-$ Mono	CD68, MNDA, CD14
$CD16^+$ Mono	CD68, MNDA, CD14, FCGR3A
cDC	CD68, MNDA, CD1C, CLEC10A
pDC	CD68, IL3RA, CLEC4C
Granulocyte	IL3RA, CLC
$CD4^+$ T	CD3D, CD4
$CD8^+$ T	CD3D, CD8A
DNT	CD3D
NKT	CD3D, NCAM1, FCGR3A
NK	NCAM1, FCGR3A
Stem cell	CD34
Platelet	ITGA2B

Abbreviations: Mono, monocytes; cDC, conventional dendritic cell; pDC, plasmacytoid dendritic cell; DNT, double negative T cells; NKT, natural killer T cells; NK, natural killer cells.

Supplementary Table 3

Clinical characteristics, laboratory findings, and T cell subsets for patients with T1D and age- and sex-matched control subjects.

Characteristic	HD (n = 35)	New-onset (n = 21)	remission (n = 34)	Post-remission (n = 35)	*p*-value
Age	13.4 (7.5–32.0)	7.0 (3.9–29.1)	14.0 (8.7–39.7)	11.2 (4.9–33.0)	0.004*
Male, n (%)	20 (57.1)	8 (38.1)	17 (50.0)	21 (60.0)	0.231
Duration	/	0.7 (0.3–3.0)	7.4 (0.3–24.0)	22.89 (6.4–35.8)	0.000*
BMI	20.2 (14.7–24.3)	15.3 (13.6–20.9)	18.0 (14.4–22.9)	16.8 (10.6–26.7)	0.000*
SCP	1313.6 (362.2–2606.6)	249.5 (34.1–299.7)	547.0 (319.9–1120.6)	133.4 (16.5–291.2)	0.000*
HbA1c (%)	5.5 (5.1–5.9)	8.4 (6.2–15.2)	6.8 (5.8–8.5)	7.2 (5.6–9.4)	0.000*
HbA1c (mmol/mol)	36.7 (32.2–41.3)	68.7 (44.7–142.2)	51.3 (40.2–69.2)	55.2 (37.4–79.5)	0.000*
GADA	/	0.2146 (−0.0054–1.0171)	0.1800 (−0.0228–1.5461)	0.0666 (−0.0151–1.8098)	0.198
IA2A	/	0.0167 (−0.0038–1.2864)	0.8309 (−0.0036–2.8134)	0.0889 (−0.0038–2.4476)	0.115
ZnT8A	/	0.0085 (−0.0057–1.1850)	0.0068 (−0.0083–0.6529)	0.0067 (−0.0040–0.6371)	0.808
$CCR7^+$ $TIGIT^-$ Treg	42.6 ± 7.8	49.2 ± 9.4	39.9 ± 7.8	48.0 ± 7.1	0.000*
$CCR7^-TIGIT^+$ Treg	22.6 ± 6.2	14.2 ± 7.5	20.5 ± 4.9	14.0 ± 5.1	0.000*
$CD226^+CCR7^-$ $CD8^+$ T cells	57.0 ± 5.9	67.0 ± 6.8	57.0 ± 7.9	70.8 ± 6.6	0.000*
$TIGIT^+CCR7^-$ $CD8^+$ T cells	60.5 ± 14.3	55.6 ± 12.8	63.7 ± 12.6	55.5 ± 13.3	0.060

Values represent the number of patients, median (minimum ~ maximum) or the mean ± standard deviation, as indicated. *P* values were calculated using one-way ANOVA to compare group means. **P*-values < 0.05 were considered significant. T1D, type 1 diabetes; HD, healthy donor; remission, partial remission; BMI, body mass index; SCP, stimulating C-peptide; GADA, glutamic acid decarboxylase antibody; IA-2A, protein tyrosine phosphatase autoantibody; ZnT8A, zinc transporter 8 autoantibody.

Supplementary Table 4

Multivariate logistic regression analysis to identify the variables independently associated with remission in T1D.

	Multivariate analysis			Multivariate analysis	
	Odds ratio (CI 95%)	*p*-value		Odds ratio (CI 95%)	*p*-value
Age	1.01 (0.92–1.09)	0.91	Age	1.05 90.93–1.18)	0.43
Gender	2.26 (0.71–7.18)	0.17	Gender	1.71 (0.44–6.74)	0.44
BMI	1.17 (0.93–1.46)	0.19	BMI	1.27 (0.95–1.69)	0.11
$CCR7^{+}TIGIT^{-}$ Treg	0.86 (0.78–0.04)	0.00	$CD226^{+}$ $CCR7^{-}CD8^{+}$ T cells	0.74 (0.65–0.86)	0.00
Age	1.04 (0.95–1.14)	0.43	Age	1.07 (0.98–1.16)	0.11
Gender	1.52 (0.47–4.92)	0.46	Gender	1.74 (0.62–4.87)	0.29
BMI	1.06 (0.85–1.33)	0.61	BMI	1.10 (0.89–1.37)	0.39
$CCR7^{-}TIGIT^{+}$ Treg	1.31 (1.15–1.48)	0.00	$TIGIT^{+}$ $CCR7^{-}CD8^{+}$ T cells	1.06 (1.01–1.10)	0.01

The model includes 90 patients; 34/90 (37.8%) patients are in the remission phase. *P* values were calculated using Wald tests from the multivariate logistic regression model. T1D, type 1 diabetes; remission, partial remission; BMI, body mass index; Gender is a dichotomous variable; all other variables are continuous.

Supplementary Table 5 Clinical characteristics and laboratory findings of patients with T1D in the discovery cohort.

Characteristic	Overall, N = 70[1]	Group Slow, N = 34[1]	Fast, N = 36[1]	*p*-value[2]
Sex				0.494
Male	42 (60%)	19 (56%)	23 (64%)	
Female	28 (40%)	15 (44%)	13 (36%)	
Age	12.00 (8.70, 16.93)	13.54 (11.36, 17.38)	10.25 (7.99, 15.85)	0.055
BMI	17.42 (16.20, 19.83)	17.42 (15.76, 19.68)	17.44 (16.47, 20.00)	0.681
Duration	1.55 (0.68, 3.24)	1.22 (0.47, 2.58)	1.65 (1.03, 3.33)	0.147
FCP	134.20 (71.73, 221.43)	127.10 (75.73, 197.58)	148.90 (68.23, 233.93)	0.613
PCP	418.50 (220.98, 614.55)	421.20 (200.68, 553.60)	414.65 (222.33, 626.48)	0.711
CP-AUC	523.65 (305.98, 829.48)	481.95 (293.60, 716.93)	564.10 (324.58, 880.10)	0.626
HbA1c (%)	7.80 (6.90, 11.15)	9.05 (6.98, 12.88)	7.65 (6.63, 9.18)	0.068
HbA1c (mmol/mol)	61.75 (51.91, 98.36)	75.41 (52.73, 117.21)	60.11 (48.91, 76.78)	0.068
GAD-A	0.31 (0.05, 1.18)	0.29 (0.04, 1.04)	0.33 (0.05, 1.23)	0.823
IA-2A	0.42 (0.04, 1.66)	0.26 (0.02, 1.53)	0.81 (0.16, 1.70)	0.231
ZnT8-A	0.05 (0.00, 0.24)	0.06 (0.00, 0.14)	0.05 (0.00, 0.29)	0.814
Number				0.045
1	17 (24%)	12 (35%)	5 (14%)	
2	30 (43%)	10 (29%)	20 (56%)	
3	23 (33%)	12 (35%)	11 (31%)	
TDD (u/kg)	0.52 (0.32, 0.61)	0.55 (0.28, 0.61)	0.50 (0.37, 0.61)	0.865

[1]n (%); Median (IQR)

[2]Pearson's Chi-squared test; Wilcoxon rank sum test (two-tailed)

P-values < 0.05 were considered significant. T1D, type 1 diabetes; BMI, body mass index; FCP: fasting C-peptide; PCP, postprandial C-peptide; GADA, glutamic acid decarboxylase antibody; IA-2A, protein tyrosine phosphatase autoantibody; ZnT8A, zinc transporter 8 autoantibody; TDD: total daily dose of insulin.

Supplementary Table 6

Clinical characteristics and laboratory findings of patients with T1D in the validation cohort.

Characteristic	Group			*p*-value[2]
	Overall, N = 40[1]	Slow, N = 27[1]	Fast, N = 13[1]	
Sex				0.314
Male	17 (43%)	10 (37%)	7 (54%)	
Female	23 (58%)	17 (63%)	6 (46%)	
Age	12 (8, 18)	15 (10, 21)	8 (7, 10)	0.001
BMI	16.7 (15.5, 19.2)	17.7 (15.9, 20.1)	15.7 (15.5, 16.6)	0.083
Duration	1.90 (0.63, 3.55)	1.50 (0.45, 3.67)	2.67 (1.93, 3.27)	0.133
FCP	105 (64, 188)	111 (63, 176)	88 (66, 239)	0.977
PCP	219 (114, 490)	233 (112, 457)	151 (133, 555)	0.931
CP-AUC	308 (198, 691)	336 (198, 671)	271 (217, 831)	0.954
HbA1c (%)	10.82 ± 3.08	11.56 ± 2.90	9.16 ± 2.91	0.027
HbA1c (mmol/mol)	95 ± 34	103 ± 32	77 ± 32	0.027
GAD-Ab	0.19 (0.03, 0.71)	0.36 (0.07, 0.89)	0.05 (0.01, 0.18)	0.050
IA-2A	0.38 (0.02, 1.08)	0.23 (0.02, 0.97)	0.38 (0.18, 1.48)	0.341
ZnT8-Ab	0.01 (0.00, 0.11)	0.00 (0.00, 0.09)	0.11 (0.03, 0.30)	0.069
Number				0.484
1	13 (33%)	3 (23%)	10 (37%)	
2	27 (68%)	10 (77%)	17 (63%)	
3	0 (0%)	0 (0%)	0 (0%)	
TDD (u/kg)	0.48 (0.34, 0.74)	0.56 (0.38, 0.73)	0.36 (0.32, 0.74)	0.326

[1]n (%); Median (IQR); Mean ± SD

[2]Pearson's Chi-squared test; Wilcoxon rank sum test; Welch Two Sample t-test (two-tailed)

P-values < 0.05 were considered significant. T1D, type 1 diabetes; BMI, body mass index; FCP: fasting C-peptide; PCP, postprandial C-peptide; GADA, glutamic acid decarboxylase antibody; IA-2A, protein tyrosine phosphatase autoantibody; ZnT8A, zinc transporter 8 autoantibody; TDD: total daily dose of insulin.

Supplementary Table 7

Clinical characteristics and laboratory findings of patients with T1D in the prediction cohort of Treg subsets.

Characteristic	Group			*p*-value[2]
	Overall, N = 60[1]	Slow, N = 35[1]	Fast, N = 25[1]	
Sex				0.221
Male	28 (47%)	14 (40%)	14 (56%)	
Female	32 (53%)	21 (60%)	11 (44%)	
Age	12 (8, 19)	15 (9, 21)	9 (7, 13)	0.006
BMI	17.20 (15.52, 19.52)	17.70 (15.58, 20.14)	16.49 (15.52, 18.02)	0.301
Duration	2.0 (0.6, 4.0)	1.4 (0.4, 3.7)	2.8 (1.6, 4.3)	0.077
FCP	117 (63, 192)	111 (59, 168)	131 (66, 196)	0.653
PCP	228 (151, 451)	233 (112, 407)	186 (151, 555)	0.631
CP-AUC	324 (200, 670)	348 (198, 586)	285 (217, 810)	0.686
HbA1c (%)	10.81 ± 2.99	11.56 ± 2.76	9.61 ± 3.01	0.019
HbA1c (mmol/mol)	95 ± 33	103 ± 30	82 ± 33	0.019
GAD-Ab	0.21 (0.03, 0.77)	0.32 (0.07, 0.89)	0.08 (0.02, 0.60)	0.187
IA-2A	0.28 (0.01, 1.11)	0.14 (0.01, 0.97)	0.51 (0.01, 1.21)	0.392
ZnT8_Ab	0.02 (0.00, 0.12)	0.01 (0.00, 0.09)	0.05 (0.01, 0.24)	0.023
Number				0.524
1	23 (38%)	15 (43%)	8 (32%)	
2	22 (37%)	13 (37%)	9 (36%)	
3	15 (25%)	7 (20%)	8 (32%)	
TDD (u/kg)	0.41 (0.34, 0.69)	0.55 (0.38, 0.73)	0.37 (0.30, 0.51)	0.060

[1]n (%); Median (IQR); Mean ± SD.

[2]Pearson's Chi-squared test; Wilcoxon rank sum test; Welch Two Sample t-test (two-tailed). *P*-values < 0.05 were considered significant. T1D, type 1 diabetes; BMI, body mass index; FCP: fasting C-peptide; PCP, postprandial C-peptide; GADA, glutamic acid decarboxylase antibody; IA-2A, protein tyrosine phosphatase autoantibody; ZnT8A, zinc transporter 8 autoantibody; TDD: total daily dose of insulin.

Supplementary Table 8

Lists of all antibodies used during this study.

Antigen	Flurochorme	Clone	Vendor	Catalog#	Dilution
CD4	PerCP-Cy5.5	SK3	BioLegend	980810	1:20
CD25	BB515	2A3	BD Pharmingen	564467	1:20
CD127	PE	A109D5	BioLegend	986002	1:20
CCR7	PE-Cy7	G043H7	BioLegend	353226	1:20
TIGIT	BV785	A15153G	BioLegend	372736	1:20
CD4	PerCP-Cy5.5	SK3	BioLegend	980810	1:20
CD25	BB515	2A3	BD Pharmingen	564467	1:20
CD127	PE	A109D5	BioLegend	986002	1:20
CCR7	PE-Cy7	G043H7	BioLegend	353226	1:20
TIGIT	BV785	A15153G	BioLegend	372736	1:20
FOXP3	APC	PCH101	eBioscience™	15-4776-42	1:20
IL-10	BV421	JES3-9D7	BioLegend	501422	1:20
TGF-β1	FITC	S20006A	BioLegend	300010	1:20
granzyme B	BV510	GB11	BD Pharmingen	563388	1:20
KI67	BV650	B56	BD Pharmingen	563757	1:20
CD4	FITC	SK3	BioLegend	980802	1:20
CD8	BB700	G42-8	BD Pharmingen	745850	1:20
CCR7	PE-Cy7	G043H7	BioLegend	353226	1:20
CD226	APC	11A8	BioLegend	338311	1:20
CD4	FITC	SK3	BioLegend	980802	1:20
CD8	BB700	G42-8	BD Pharmingen	745850	1:20
CCR7	PE-Cy7	G043H7	BioLegend	353226	1:20
CD226	APC	11A8	BioLegend	338311	1:20
TIGIT	BV785	A15153G	BioLegend	372736	1:20
CD127	PE	A019D5	BioLegend	986002	1:20
CD62L	Brilliant Violet 510™	DREG-56	BD Pharmingen	563203	1:20
CTLA-4	Brilliant Violet 711™	BNI3	BioLegend	369632	1:20
CD4	FITC	SK3	BioLegend	980802	1:20
CD8	BB700	G42-8	BD Pharmingen	745850	1:20
CCR7	PE-Cy7	G043H7	BioLegend	353226	1:20
CD226	APC	11A8	BioLegend	338311	1:20
TIGIT	BV785	A15153G	BioLegend	372736	1:20
TNF	PE/Dazzle™ 594	MAb11	BioLegend	502946	1:20

IL-17A	PE	SCPL1362	BD Pharmingen	560436	1:5
granzyme B	BV510	GB11	BD Pharmingen	563388	1:20
CD226	Monoclonal antibody	10E5	Thermo Fisher	16-2261-85	
CD4	FITC	GK1.5	BioLegend	100405	1:20
CD8	AF700	53-6.7	BioLegend	100730	1:20
CD226	BV605	TX42.1	BioLegend	133613	1:40
TIGIT	PE	1G9	BioLegend	142103	1:20
CD25	BV711	PC61	BioLegend	102049	1:160
CD127	APC-Cy7	A7R34	BioLegend	135040	1:80
CCR7	PE-Cy7	4B12	BioLegend	120124	1:20
Ki-67	BV650	11F6	BioLegend	151215	1:80
IFN-r	PE-Cy7	XMG1.2	BD Pharmingen	557649	1:160
IL-17A	APC	TC11-18H10.1	BioLegend	506916	1:80
Granzyme B	BV421	QA18A28	BioLegend	396414	1:20